NANO LETTERS

pubs.acs.org/NanoLett

Direct Chemical Vapor Deposition of Graphene on Dielectric Surfaces

Ariel Ismach,[†,‡] Clara Druzgalski,[†] Samuel Penwell,[†] Adam Schwartzberg,[†] Maxwell Zheng,[†,‡] Ali Javey,[†,‡] Jeffrey Bokor,[†,‡] and Yuegang Zhang*[,†]

[†]The Molecular Foundry, Lawrence Berkeley National Laboratory, 1 Cyclotron Road, Berkeley, California 94720 and [‡]Electrical Engineering and Computer Science Department, University of California at Berkeley, Berkeley California 94720

ABSTRACT Direct deposition of graphene on various dielectric substrates is demonstrated using a single-step chemical vapor deposition process. Single-layer graphene is formed through surface catalytic decomposition of hydrocarbon precursors on thin copper films predeposited on dielectric substrates. The copper films dewet and evaporate during or immediately after graphene growth, resulting in graphene deposition directly on the bare dielectric substrates. Scanning Raman mapping and spectroscopy, scanning electron microscopy, and atomic force microscopy confirm the presence of continuous graphene layers on tens of micrometer square metal-free areas. The revealed growth mechanism opens new opportunities for deposition of higher quality graphene films on dielectric materials.

KEYWORDS Graphene, CVD, nanoelectronics

Graphene is a two-dimensional material that has been attracting extensive scientific interest. The existence of single-layer graphene was not considered possible until the recent achievement of the mechanical cleavage of highly ordered pyrolytic graphite (HOPG).[1] Since then, the extraordinary electronic properties of graphene, such as ballistic transport over ~0.4 μm length,[1] high electron mobility,[1] quantum-hall effect at room temperature,[2,3] and single-molecule field-effect sensitivity,[4] have been experimentally observed. Semiconducting graphene nanoribbons have also been fabricated to demonstrate the high performance of graphene field-effect transistors.[5,6] Application of graphene-based devices utilizing its superior electronic properties, however, requires a method of forming uniform single-layer graphene film on dielectric substrates on a large scale. The mechanical cleavage method can only lead to small areas covered with graphene and is thus not suitable for large-scale fabrication processes. The ultrahigh vacuum annealing of single-crystal SiC (0001)[7,8] may lead to better coverage but with relatively small domain size and requiring expensive materials and equipment. Continuous films have been achieved by chemical routes, such as deposition from solution-based exfoliated graphite[9,10] and graphite oxide.[11,12] Such approaches, however, lack control of the number of graphene layers and exhibit deteriorated transport properties. Catalytic chemical vapor deposition (CVD) on single-crystal transition metals has also been shown to lead to relatively high coverage of high quality graphene.[13−16] However, the expensive substrates inhibit the use of this method in large-scale processes. Recently, less expensive and more accessible methods for CVD synthesis of high quality large area graphene were demonstrated using polycrystalline nickel films[17,18] and copper foils[19,20] or copper film.[21] The graphene film could be transferred to various substrates after etching off the metals.[17−20] A non-CVD synthesis of relatively large number of graphene layers (mainly 5−10 layers) was also achieved by dissolution of a solid carbon source in a nickel film and subsequent segregation of graphene on a silion dioxide substrate.[22] Use of metal with high carbon solubility such as nickel, however, normally has difficulty to control the number of graphene layers, no matter if the method is based on CVD[17,18] or solid state diffusion.[22] A method for direct CVD growth of only few-graphene layers on nonconducting materials is much needed for future electronic and optical applications. The study of such direct deposition process is also scientifically intriguing for understanding the graphene CVD growth mechanism.

Here we present a method for the direct chemical vapor deposition of a single- or few-layer graphene film on dielectric surfaces via a sacrificial copper film. Following recent reports, we have been working on the CVD growth of graphene on metals,[17,18,20] and on micrometer-thick copper foils in particular, noticing that a significant amount of the copper evaporates and deposits at the edges of the fused silica tube used in the CVD (see SI for growth methods). Considering the melting temperature of the copper, ~1084 °C, along with the high temperature during the growth, ~1000 °C, and the low pressure in the chamber, 100−500 mTorr, the significant evaporation of the metal is not surprising. Based on this observation, we propose a mechanism for in situ graphene deposition on insulating surfaces by a controlled metal evaporation from the surfaces during, or immediately after, the catalytic growth (Figure 1). The use

* To whom correspondence should be addressed. E-mail: yzhang5@lbl.gov.
Received for review: 08/31/2009
Published on Web: 04/02/2010

© 2010 American Chemical Society

DOI: 10.1021/nl9037714 | *Nano Lett.* **2010,** *10,* 1542–1548

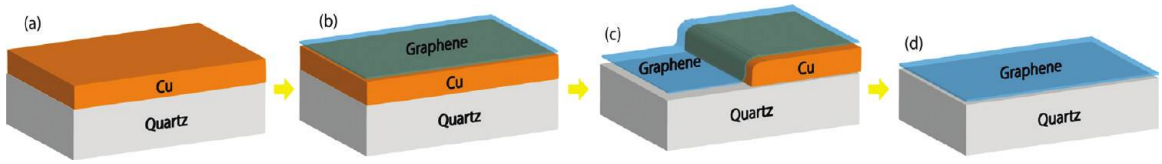

FIGURE 1. Schematic representation of the process. First a thin layer of copper is evaporated on the dielectric surface, (a). During the CVD, (b), the metal dewets and evaporates, (c), leaving the graphene layer on the substrate (d).

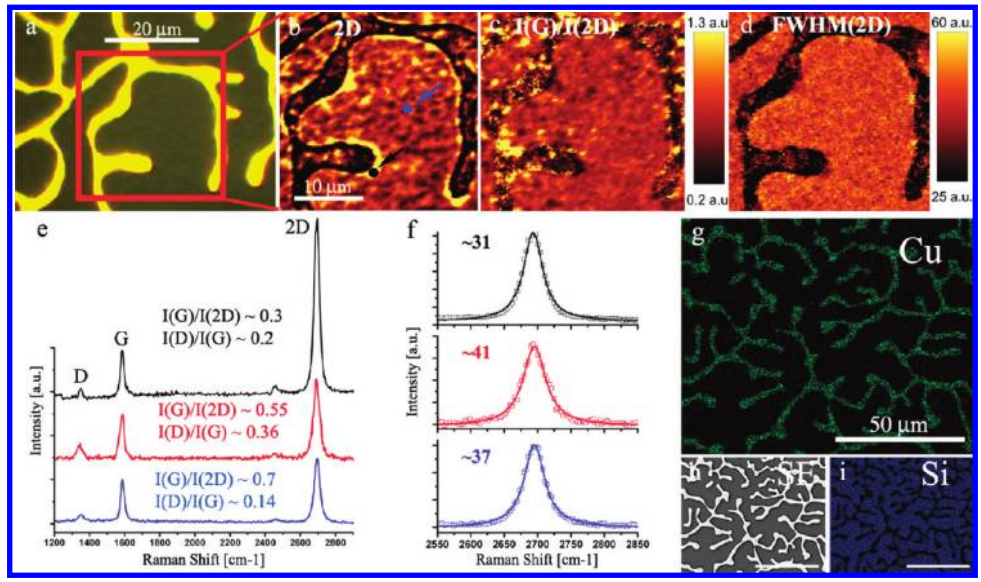

FIGURE 2. Sample characterization. (a) Optical microscope image of a sample with 450 nm Cu after 2 h CVD, showing the finger morphology of the metal. (b) Scanning Raman 2D band mapping of a continuous graphene film between the metal fingers, over the area marked by the red square in (a). (c,d) Mapping of I(G)/I(2D) and FWHM(2D) of the same area in (b), respectively. (e) The Raman spectra from three different points marked in (b) by the colored arrows and dots, and their respective I(G)/I(2D) and I(D)/I(G) ratios. (f) Lorentzian curve fitting to the 2D band in the different spots in (b,e), with their respective FWHMs. (g) Cu mapping in EDX analysis confirms the absence of Cu between the fingers. (h) SEM image of the same area with the secondary electrons (SE) detector. (i) Si (from the quartz substrate) mapping in EDX analysis of the same area.

of copper as a low carbon solubility metal catalyst should enable a better control on the number of layers.[19−21]

To experimentally demonstrate our method, we first use electron-beam evaporation to deposit copper (Cu) films 100 to 450 nm in thickness on a variety of substrates (single-crystal quartz, sapphire, silicon wafers with 300 nm thermal SiO_2, and fused silica). We then perform CVD using these substrates with durations varying from 15 min up to 7 h at 1000 °C (See SI for details). This allows us to study the effect of film thickness, substrate type, and CVD growth time on the graphene formation. The samples are characterized by Raman spectroscopy (Witec, 532 nm laser), which is a powerful and well recognized method for the characterization of graphitic materials[23,24] and allows for the identification of single and few-layer graphene.[23−25] Other characterization methods include scanning electron microscopy (SEM, Zeiss Gemini Ultra-55), energy-dispersive X-ray spectroscopy (EDX, Zeiss Gemini Ultra-55), optical microscopy (Leica DM4000), and atomic force microscopy (AFM, Digital Instruments 3000).

Figure 2a shows an optical image of a typical sample with a 450 nm thick Cu film on single-crystal quartz after 2 h CVD growth. The dewetting of the metal into fingerlike structures can be appreciated. Raman spectroscopy was used to detect and characterize the presence of graphene in metal-free areas. The scanning Raman image of the signature graphene 2D band is shown in Figure 2b. The mapping with the ratio I(G)/I(2D) and the full width half-maximum of the 2D band, FWHM(2D), are shown in Figure 2 panels c and d, respectively. The Raman spectra displayed in Figure 2e correspond to the black, red, and blue dots and arrows in Figure 2b and show the typical signature of single- or few-layer graphene,[17,24−27] that is, small values for the ratio I(G)/I(2D) $\approx 0.3-0.7$ (Figure 2e), the single and sharp Lorentzian peak shape of the 2D band and the FWHM(2D) $\approx 31-41$ cm^{-1} (see the curve fitting in Figure 2f, the FWHM(2D) values are written in the top left of each peak). These Raman results are very similar to previous reports on graphene grown on SiC[26,28−30] and on metal films by CVD,[17,26] and will be further discussed later in the paper. The areas in between the metal fingers vary in size and shape with the thickness of the metal and duration of the CVD process. In general, $\sim 20\,\mu$m^2 size areas filled with continuous graphene layers are easily achieved, as shown in Figure 2b by the continuous 2D band signal distribution. In addition to the major G and 2D bands, a weaker D-band is also detected in most of the scanned areas.

© 2010 American Chemical Society

DOI: 10.1021/nl9037714 | Nano Lett. 2010, 10, 1542--1548

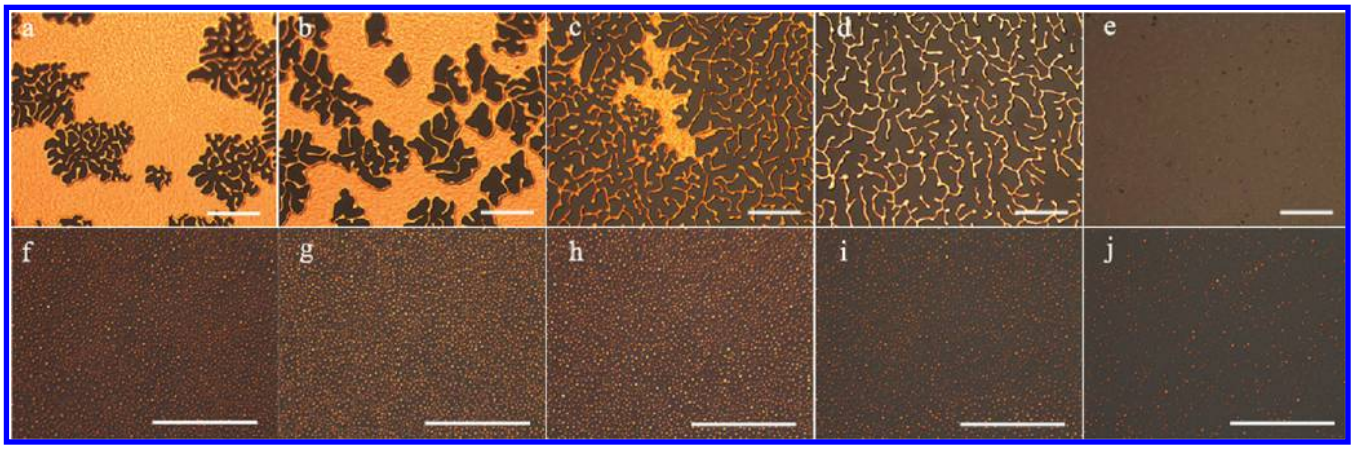

FIGURE 3. Dewetting and evaporation evolution with the CVD time. (a−e) Optical micrographs showing the morphology evolution of the metal with the increasing of CVD time for 15, 30, 60, 120, and 420 min, respectively, for a 450 nm thick Cu film. (f−j) The same for a 100 nm Cu film, except for (j) where 300 min CVD time is used.

This band is not present in high quality graphitic materials and needs a disorder or defect in the lattice to be activated,[23,24,26] such as point defects, subdomain boundaries, and edges,[23,24,26] suggesting that the deposited graphene is of lower quality than the samples prepared by exfoliation of HOPG.[25]

CVD-derived few-layer graphene exhibits the characteristics similar to that of turbostratic graphene, that is, lack of long order in the *c* direction. In contrary, most of the reported Raman data using few exfoliated HOPG layers tend to keep the highly ordered structure of graphite. In the latter, single-layer can be differentiated from the bilayer and trilayer graphene by the shape of the 2D band. In exfoliated bilayer graphene, the 2D band can be fitted with four Lorentzians,[23−26] while monolayer graphene has a single and sharp Lorenztian peak.[23−26] On the other hand, on CVD-derived few graphene layers on SiC[26,28−30] and metal surfaces[17,26] one, two, and three layer graphene samples all exhibit a single and sharp Lorentzian-shaped peak, comparable to results in turbostratic graphite.[23,24,26,28,31] The reason for that is believed to be the lack of order in the *c* axis compared to the ordered AB stacking in HOPG crystals,[17,26−29] and the electronic coupling between the layers is not homogeneous, having areas with strong and weak coupling. Thus, the line shape of the 2D peak alone is not enough to identify the number of layers in CVD grown graphene. Kong and coauthors[17] used a combination of AFM and Raman spectroscopy to show that the I_G/I_{2D} ratio provides a good estimation of the number of layers in their graphene samples. Applying the same principle, we determined that our samples consist of 1−3 graphene layers.

SEM and EDX characterization are performed to confirm the dewetting of the metal and the presence of graphene on metal-free zones, as shown in Figure 2g, where the elemental mapping of Cu (green) is shown to reproduce the finger shape of the metal on quartz as shown in the optical microscope image (Figure 2a). The secondary electron image of the same area is shown in Figure 2h and the silicon elemental mapping in Figure 2i. Additional EDX mapping images are shown in the Supporting Information (Figure SI1). The best direct deposition of graphene results were obtained on quartz and M-plane sapphire. However it was also shown possible on SiO_2 (300 nm)/silicon wafer and fused silica. Some of these results are summarized in Supporting Information Figure SI3.

The continuity of the metal film on the surface depends on its thickness, the metal-dielectric wetting properties, and the heating temperature and time. Figure 3 shows the dewetting/evaporation evolution for 450 and 100 nm thick Cu films on quartz, respectively. After the initial heating, the dewetting and evaporation rates of the metal decreased, presumably, due to the graphene growth that increased its coverage of the copper surface.[20] For the 450 nm Cu films, coexistence of continuous Cu areas and fingerlike structures can be seen after 15−30 min CVD (Figure 3a,b). The film breaks completely into fingers after ∼2 h of growth (Figure 3d); however, an additional 5 h are required to entirely evaporate the metal (Figure 3e). For the 100 nm Cu samples, the film instability is more pronounced. The metal film breaks into submicrometer dots in less than 15 min of CVD, however most of the remaining Cu evaporates only after 5 h of CVD growth, as shown in Figures 3f−j (Complete Cu evaporation occurs after ∼3 h heating in control experiments without graphene growth, not shown). The dewetting evolution results of 300 nm thick films on quartz, M-plane sapphire, and SiO_2/Si are shown in Supporting Information Figure SI4. Occasionally, the dewetting of the metal prior to the CVD (during temperature ramping-up) is also observed on samples with 450 nm Cu and is the cause for the discontinuity of the graphene layer in some metal-free areas; see Supporting Information Figures SI6 and SI7. Since only an initially continuous metal catalyst film may lead to large area coverage with graphene (Figures 2b and Supporting Information SI5), the metal film thickness should be greater than or equal to 450 nm, on quartz, for continuous graphene film growth under the current CVD conditions (see Supporting Information for details). Thinner metal films break into

© 2010 American Chemical Society

DOI: 10.1021/nl9037714 | *Nano Lett.* **2010,** *10,* 1542--1548

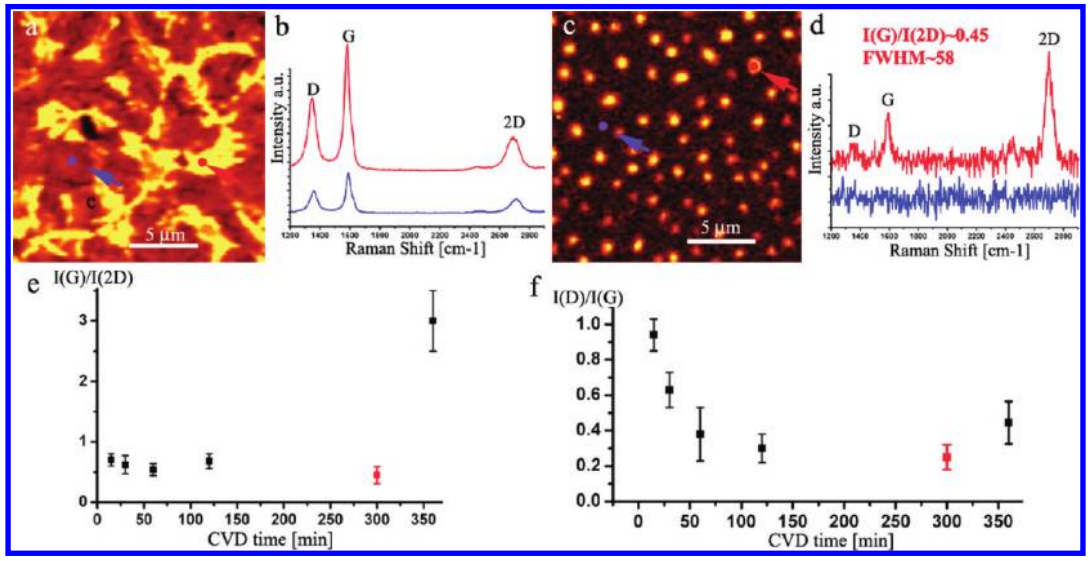

FIGURE 4. Raman characterization of extreme CVD conditions. (a) Graphene 2D band Raman mapping of a 450 nm thick Cu sample after 6 h CVD. The Raman spectra show a continuous defective graphitic layer, (b−d) The Raman 2D band mapping and spectra of a 100 nm thick copper film sample after 5 h CVD. The red and blue spectra correspond to the bright and dark areas in the Raman map, respectively, showing very clearly the selective presence of graphene on the bright dots. (e) The evolution of the area-averaged *I*(G)/*I*(2D) ratio with the CVD time for a 450 nm Cu/quartz sample (black) and for a 100 nm Cu/quartz sample (red), showing no significant change from 15 to 120 min of growth time. (f) The area-averaged *I*(D)/*I*(G) as a function of growth time for a 450 nm Cu/quartz sample (black) and for 100 nm Cu/quartz sample (red). The drop in the ratio values for a 450 nm Cu/quartz sample (black) suggests a continuous improvement of the graphene quality with the CVD time up to 120 min, before deterioration for longer CVD time (6−7 h).

fingers or dots during temperature ramping-up before the CVD starts (see Supporting Information Figure SI5 for 300 nm Cu films and Figures 3f−j for 100 nm Cu films), resulting in large uncovered areas.

In order to further understand the growth mechanism, we investigated the Raman characterization of two samples obtained under extreme experimental conditions (Figure 4). The scanning Raman image of the graphene 2D band on a 450 nm Cu film sample after 6 h CVD growth (Figure 4a, the optical microscope image of a similar sample is shown in Figure 3e), exhibits a continuous carbon film on the bare dielectric surface. However, unlike the high-quality single or few-layer graphene film in Figure 2, the film here is highly defective and composed of thicker graphitic-like material or highly damaged graphene layers[32] (see the Raman spectra in Figure 4b). Although the reason for this difference is still unclear, one possibility is that the grown graphene layers break under stress due to the Cu morphology change during its evaporation and expose the underlying metal to further catalyst reaction, which results in an increasing number of defects and graphene layers. It might also arise from Cu residues on the surface and by Cu redeposition on top of the graphene under the extreme CVD condition. On the other hand, the scanning Raman image with the 2D band in Figure 4c shows that samples with 100 nm thick Cu films after 5 h growth lead to the deposition of discrete submicrometer graphene dots on bare quartz substrates, following the initial Cu dot pattern spontaneously formed during initial heating (see the optical microscope image in Figures 3f−j). The respective spectra from the graphene (bright) dots and bare substrate (dark) regions are shown in Figure 4d and Supporting Information SI4, confirming the presence of graphene only on the dots.

Figures 4e,f show the averaged ratio *I*(G)/*I*(2D) and *I*(D)/*I*(G) as a function of the CVD growth time for 450 nm thick Cu films on quartz (black symbols, the red square is from the graphene dots of the 100 nm Cu sample in Figures 4c,d). The averaged ratio *I*(G)/*I*(2D) exhibits only minor change up to 2 h growth and remains at ∼0.68 and then climbs to ∼3 for 6 h growth. On the other hand, area-averaged *I*(D)/*I*(G) drops from ∼0.9 to ∼0.3 for 15 min and 2 h growths, respectively, followed by an increase to ∼0.45 for longer growth time (6 h). The ratio between the intensities of the D and G bands, *I*(D)/*I*(G), is considered to be proportional to the amount of structural defects and inversely proportional to the domain size in graphitic materials.[23,24] The initial decrease of the *I*(D)/*I*(G) may be attributed to the increase in film continuity and the formation of larger domains with longer growth time. Interestingly, during the first 2 h of growth, no significant change in the ratio *I*(G)/*I*(2D) is measured, suggesting that the number of layers and the stacking order in the deposited graphene is independent of the CVD time within a 2 h range. However, both graphs in Figures 4e,f show that prolongated growth time for the 450 nm Cu samples has a dramatic influence in the graphene quality, stacking order, and defects, as also appreciated in Figures 4a,b. As already mentioned above, the change in the graphene layer under this extreme condition may be due to stress-induced broken graphene films and the nucleation of new graphene layers at the exposed Cu sites, increasing the number of layers and reducing the domain size, L_a. The narrow D, G, and 2D bands in our samples suggest our film

© 2010 American Chemical Society

DOI: 10.1021/nl9037714 | *Nano Lett.* **2010,** *10,* 1542--1548

is in the crystalline or nanocrystalline regime. In this case,[33] L_a can be estimated using the so-called Tuinstra-Koenig (TK)[33−36] relation, L_a (nm) = $C(\lambda)[I(D)/I(G)]^{-1}$. The averaged $I(D)/I(G)$ ratio is calculated from the Raman data, and the $C(532\ nm) = 4.95$ nm was calculated using the correction in ref 37. We found L_a value is ∼5.5 nm for 15 min growth, increasing to ∼16.5 nm after 2 h growth, and shrinking back to ∼12 nm after 6−7 h growth, presumably due to the increasing number of layers and cracks during the final stages of metal dewetting. On some locations, domain sizes of up to ∼35 nm were found on 450 nm Cu on quartz after 2 h CVD (see the blue spectra in Figure 2e). All the calculations were done with Raman data from continuous graphene films and assuming D band arises mainly from domain boundaries. The calculated values may be lower than the actual L_a due to the existence of other defects. Ferrari and coauthors[33] also pointed out that the TK equation underestimate the size of the crystal domains in graphitic samples because it assumes a uniform domain size, as opposed to XRD methods that are more sensitive to the larger domains. Thus, a larger domain size should be expected in our samples. It should be noted that the influence of CVD time on the graphene film quality is highly dependent on the other parameters, such as the Cu film thickness. On the 100 nm Cu sample (Figures 4c,d and the red square in f), the spectra and the relatively low area-averaged ratio $I(D)/I(G) \sim 0.25 \pm 0.07$ suggest the presence of graphene layers on the substrate with domain size of ∼20 nm on the dots (however, in this case, contribution from the graphene dot edges is expected due to the comparable size of the dots and the laser spot ∼300 nm and thus the domain size calculation is not accurate[37]). This result provides a clue for further improvement of the quality of directly deposited graphene by controlling the Cu supply and dewetting/evaporation process.

Further topographic characterization of the graphene films on the substrates reveals a more complex picture of the graphene deposition process than that illustrated in Figure 1. The SEM images, using an in-lens detector, in Figures 5a,c clearly show that there is wrinkle-like contrast in the continuous graphene film between Cu fingers. These wrinkles are not seen in SEM images using a secondary electron (SE) detector (Figures 5b,d). We know that the in-lens detector is very sensitive to surface charges while the SE detector is sensitive to topography. Thus, the graphene layer is seen clearly in the first but hardly in the latter (only the highly corrugated structure near the metal is detected, Figure 5d and Supporting Information SI7), suggesting that even the wrinkled graphene layer is very thin. The wrinkles follow the dewetting shape of the metal (also see Supporting Information Figure SI7). Figures 5c,d also show portions of suspended graphene layers bridging between the bottom substrate surface and the raised Cu finger edge (indicated by the white arrows in Figures 5b,d). AFM height images in Figures 5e,f and SI6 also confirm the quasi-periodic wrinkle structure in the corrugated graphene layer. The wrinkles

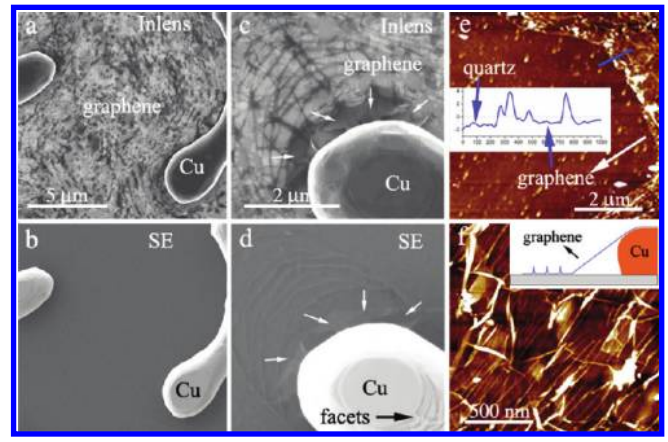

FIGURE 5. SEM and AFM characterization. (a) SEM image with an in-lens detector, showing a continuous graphene film between the metal fingers. The wrinkles following the shape of the metal can be easily observed. (b) The same area as in (a) but imaged with a SE detector; the graphene is hardly observed. (c,d) The same as in (a) and (b) with higher magnification. In these SEM images, suspended graphene sheets (white arrows) are observed near the metal edge. On the flat surface, however, only the highly corrugated graphene areas on the surface are seen in (d). (e) AFM height image showing a noncontinuous graphene layer. The inset shows the height profile along the blue line, showing that the layer is ∼0.8 nm height. (f) AFM height image of a continuous graphene area with quasi-periodic wrinkles. The inset shows a schematic representation of the graphene deposit.

have a typical separation of ∼40−120 nm and height 1−5 nm, in contrast with the graphene film height of ∼0.8−1.2 nm (see Figure 5e and Supporting Information SI6). One possible mechanism for the wrinkle formation is the stress-induced graphene sheet rupture and the subsequent new graphene nucleation at the ruptured sites during the Cu receding process. The surface reconstruction (e.g., facet formation at high temperature, see Figure 5d) of Cu or the substrate could be another possible reason.

On the basis of the observed topographic features of the directly deposited graphene, we may now have a further discussion on the Raman data. The Raman spectra near the Cu edge (such as the black in Figure 2e) give an average FWHM(2D) of 30 ± 5 cm^{-1}, an $I(G)/I(2D)$ ratio of ∼0.3 ± 0.06, and an $I(D)/I(G)$ ratio of 0.2 ± 0.08, indicating a single-layer graphene. On the other hand, the Raman spectra from the metal-free areas (such as the blue and red in Figure 2e, and red in Figure 4d) give an average 2D band FWHM of 45 ± 5 cm^{-1}, an $I(G)/I(2D)$ ∼0.68 ± 0.1, and an $I(D)/I(G)$ ratio of ∼0.3 ± 0.06 (120 min CVD in Figures 4e,f), characteristics of a 1−3 graphene layers.[17,23,24,26] Interestingly, the Raman spectra near the metal exhibit ∼1.5 times higher intensity values than the spectra on the surface. One possible reason for this location dependent Raman signature is that, near the metal, the graphene is mostly suspended; see Figure 5c,d and the inset in Figure 5f, and thus, the effective sampling by the laser spot of ∼300 nm in diameter on a suspended graphene from the substrate to the ∼300−500 nm height copper fingers is roughly ∼1.4 times higher calculated from simple geometrical considerations. Moreover, the suspended

© 2010 American Chemical Society

DOI: 10.1021/nl9037714 | *Nano Lett.* **2010,** *10,* 1542--1548

graphene is stretched between the substrate and the top of the metal, lacking the wrinkle structure as the graphene deposited on the substrate. The wrinkled structure of the graphene on metal-free areas may induce local strain in the layer causing the broadening of the 2D peak as shown for uniaxial strained graphene.[38] Defects, indicated by the presence of a D peak, may be another reason for the broadening of the G and 2D peaks.[39] The averaged G band position, Pos(G), and its FWHM(G) in the metal-free areas, such as in Figure 2, is about 1594 ± 2 and 34 ± 3.2 cm^{-1}, respectively. The upshift in the position (from $\sim$1580 cm^{-1}) together with the increasing of the FWHM(G) suggests that the broadening is caused mainly by defects and not by doping.[39−41] On the suspended graphene between the metal fingers and the substrate (Figure 5c,d), Pos(G) and FWHM(G) were found to be $\sim$1587 and $\sim$22 cm^{-1}, respectively, similar to the Raman peaks (Pos(G)$\sim$1580 cm^{-1} and FWHM(G)$\sim$16 cm^{-1}) for intrinsic graphene.[39−41] In the case of the 2D peak, no shift was found comparing the data from the metal-free areas and suspended graphene (Pos(2D)$\sim$2700 cm^{-1}), but the FWHM(2D) is broader on the former, probably due to the strain and defects as discussed previously. On the other hand, D peak was detected on the metal-free areas and on suspended layers, so the presence of defects alone cannot explain the difference in the Raman peaks of the two different areas. These results suggest that the substrate and the wrinkled graphene morphology may play a crucial role in the broadening and relative intensity of the Raman peaks. Further study is needed to clarify the specific contribution of the substrate, defects, strain, and doping on the Raman data.

The presence of wrinkles is generally expected to have a negative effect on the electronic properties of the graphene due to the presence of strain and defects. Theoretical[42,43] and experimental[14,44] works have shown that the presence of ripples and wrinkles on the graphene creates midgap states that deteriorate the conductance being the main reason for scattering.[42−44] However, a controllable introduction of wrinkle structure in graphene could potentially modulate its electronic property in a positive way. Density functional theory predicts a local enhancement in chemical reactivity on the ripples.[45] The increased hydrogenation in single layer graphene (rippled structure) compared to the bilayer (flat),[46] may support this local enhancement in chemical reactivity. Moreover, theoretical studies show that periodic potentials (by means of periodic electric or magnetic fields, patterning of impurities/charges and defects or deformations such as wrinkles and ripples) applied to the graphene may create superlattice-like graphene structures without the needs of cutting and etching.[14,47] Our deposited wrinkled graphene and few-graphene layers may facilitate the study of such nanostructures on the electronic, mechanical, and chemical properties of graphene. However, further understanding of the roles of CVD parameters is needed to improve the control on the morphology and quality of the directly deposited graphene films on dielectric substrates.

In summary, we have demonstrated the direct growth and deposition of graphene layers on dielectric surfaces without any postetching process. This process was shown to be suitable on a variety of dielectric surfaces including single-crystal quartz, sapphire, fused silica, and silicon oxide wafers. Further improvement on the control of the dewetting and evaporation process could lead to the direct deposition of patterned graphene for large-scale electronic device fabrication. This method could also be generalized to deposit other two-dimensional materials, such as boron−nitride.

Acknowledgment. The authors thank Professor Mildred Dresselhaus and Professor Andrea Ferrari for their helpful advice with the Raman spectroscopy characterization, Drs. Shaul Aloni, Tevye Kuykendall, Jim Schuck, Jeffery Urban, and Alex Weber-Bargioni for discussion and experimental support. This work was supported by the Office of Science, Office of Basic Energy Sciences, of the U.S. Department of Energy under contract no. DE-AC02-05CH11231. A.I. and J.B. also acknowledge the support of the MSD Focus Center, one of five research centers funded under the Focus Center Research Program, a Semiconductor Research Corporation program.

Note Added after ASAP Publication. An author was added to the author list and revisions to the Acknowledgments were made in the version of this paper published ASAP April 2, 2010; the corrected version published ASAP April 16, 2010.

Supporting Information Available. A detailed description of the experimental methods and additional experimental results. This material is available free of charge via the Internet at http://pubs.acs.org.

REFERENCES AND NOTES

(1) Novoselov, K. S.; Geim, A. K.; Morozov, S. V.; Jiang, D.; Zhang, Y.; Dubonos, S. V.; Grigorieva, I. V.; Firsov, A. A. *Science* **2004**, *306* (5696), 666–669.
(2) Zhang, Y. B.; Tan, Y. W.; Stormer, H. L.; Kim, P. *Nature* **2005**, *438* (7065), 201–204.
(3) Novoselov, K. S.; Jiang, Z.; Zhang, Y.; Morozov, S. V.; Stormer, H. L.; Zeitler, U.; Maan, J. C.; Boebinger, G. S.; Kim, P.; Geim, A. K. *Science* **2007**, *315* (5817), 1379–1379.
(4) Schedin, F.; Geim, A. K.; Morozov, S. V.; Hill, E. W.; Blake, P.; Katsnelson, M. I.; Novoselov, K. S. *Nat. Mater.* **2007**, *6* (9), 652–655.
(5) Li, X. L.; Wang, X. R.; Zhang, L.; Lee, S. W.; Dai, H. J. *Science* **2008**, *319* (5867), 1229–1232.
(6) Han, M. Y.; Ozyilmaz, B.; Zhang, Y. B.; Kim, P. *Phys. Rev. Lett.* **2007**, *98* (20), 206805.
(7) Hass, J.; de Heer, W. A.; Conrad, E. H. *J. Phys.: Condens. Matter* **2008**, *20* (32), 323202.
(8) Emtsev, K. V.; Bostwick, A.; Horn, K.; Jobst, J.; Kellogg, G. L.; Ley, L.; McChesney, J. L.; Ohta, T.; Reshanov, S. A.; Rohrl, J.; Rotenberg, E.; Schmid, A. K.; Waldmann, D.; Weber, H. B.; Seyller, T. *Nat. Mater.* **2009**, *8* (3), 203–207.
(9) Tung, V. C.; Allen, M. J.; Yang, Y.; Kaner, R. B. *Nat. Nanotechnol.* **2009**, *4* (1), 25–29.
(10) Hernandez, Y.; Nicolosi, V.; Lotya, M.; Blighe, F. M.; Sun, Z. Y.; De, S.; McGovern, I. T.; Holland, B.; Byrne, M.; Gun'ko, Y. K.; Boland, J. J.; Niraj, P.; Duesberg, G.; Krishnamurthy, S.; Goodhue,

© 2010 American Chemical Society

DOI: 10.1021/nl9037714 | *Nano Lett.* **2010,** *10,* 1542–1548

R.; Hutchison, J.; Scardaci, V.; Ferrari, A. C.; Coleman, J. N. *Nat. Nanotechnol.* **2008**, *3* (9), 563–568.
(11) Li, D.; Muller, M. B.; Gilje, S.; Kaner, R. B.; Wallace, G. G. *Nat. Nanotechnol.* **2008**, *3* (2), 101–105.
(12) Dikin, D. A.; Stankovich, S.; Zimney, E. J.; Piner, R. D.; Dommett, G. H. B.; Evmenenko, G.; Nguyen, S. T.; Ruoff, R. S. *Nat.* **2007**, *448* (7152), 457–460.
(13) Starodubov, A. G.; Medvetskii, M. A.; Shikin, A. M.; Adamchuk, V. K. *Phys. Solid State* **2004**, *46* (7), 1340–1348.
(14) de Parga, A. L. V.; Calleja, F.; Borca, B.; Passeggi, M. C. G.; Hinarejos, J. J.; Guinea, F.; Miranda, R. *Phys. Rev. Lett.* **2008**, *100* (5), 056807.
(15) Coraux, J.; N'Diaye, A. T.; Engler, M.; Busse, C.; Wall, D.; Buckanie, N.; Heringdorf, F.; van Gastei, R.; Poelsema, B.; Michely, T. *New J. Phys.* **2009**, *11*, 023006.
(16) Coraux, J.; N'Diaye, A. T.; Busse, C.; Michely, T. *Nano Lett.* **2008**, *8* (2), 565–570.
(17) Reina, A.; Jia, X. T.; Ho, J.; Nezich, D.; Son, H. B.; Bulovic, V.; Dresselhaus, M. S.; Kong, J. *Nano Lett.* **2009**, *9* (1), 30–35.
(18) Kim, K. S.; Zhao, Y.; Jang, H.; Lee, S. Y.; Kim, J. M.; Kim, K. S.; Ahn, J. H.; Kim, P.; Choi, J. Y.; Hong, B. H. *Nature* **2009**, *457* (7230), 706–710.
(19) Bae, S.; Kim, H.; Lee, Y.; Xu, X.; Park, J.; Zheng, Y.; Balakrishnan, J.; Im, D.; Lei, T.; Song, Y.; Kim, Y.; Kim, K.; Ozyimaz, B.; Ahn, J.; Hong, B.; Iijima, S.; *arXiv:0912.5485v1*, 2010. Accessed Feb. 8, 2010.
(20) Li, X. S.; Cai, W. W.; An, J. H.; Kim, S.; Nah, J.; Yang, D. X.; Piner, R.; Velamakanni, A.; Jung, I.; Tutuc, E.; Banerjee, S. K.; Colombo, L.; Ruoff, R. S. *Science* **2009**, *324* (5932), 1312–1314.
(21) Levendorf, M.; Ruiz-Vargas, C.; Garg, S.; Park, J. *Nano Lett.* **2009**, *9* (12), 4479−4483.
(22) Hofrichter, J.; Szafranek, B. N.; Otto, M.; Echtermeyer, T. J.; Baus, M.; Majerus, A.; Geringer, V.; Ramsteiner, M.; Kurz, H. *Nano Lett.* **2010**, *10* (1), 36–42.
(23) Pimenta, M. A.; Dresselhaus, G.; Dresselhaus, M. S.; Cancado, L. G.; Jorio, A.; Saito, R. *Phys. Chem. Chem. Phys.* **2007**, *9*, 1276–1291.
(24) Ferrari, A. C. *Solid State Commun.* **2007**, *143* (1−2), 47–57.
(25) Ferrari, A. C.; Meyer, J. C.; Scardaci, V.; Casiraghi, C.; Lazzeri, M.; Mauri, F.; Piscanec, S.; Jiang, D.; Novoselov, K. S.; Roth, S.; Geim, A. K. *Phys. Rev. Lett.* **2006**, *97* (18), 187401.
(26) Malard, L. M.; Pimenta, M. A.; Dresselhaus, G.; Dresselhaus, M. S. *Phys. Reports* **2009**, *473* (5−6), 51–87.
(27) Poncharal, P.; Ayari, A.; Michel, T.; Sauvajol, J. L. *Phys. Rev. B* **2008**, *78* (11), 113407.
(28) Faugeras, C.; Nerriere, A.; Potemski, M.; Mahmood, A.; Dujardin, E.; Berger, C.; de Heer, W. A. *Appl. Phys. Lett.* **2008**, *92* (1), 011914.
(29) Hass, J.; Varchon, F.; Millan-Otoya, J. E.; Sprinkle, M.; Sharma, N.; De Heer, W. A.; Berger, C.; First, P. N.; Magaud, L.; Conrad, E. H. *Phys. Rev. Lett.* **2008**, *100* (12), 125504.
(30) Lee, D. S.; Riedl, C.; Krauss, B.; von Klitzing, K.; Starke, U.; Smet, J. H. *Nano Lett.* **2008**, *8* (12), 4320–4325.
(31) Cancado, L. G.; Takai, K.; Enoki, T.; Endo, M.; Kim, Y. A.; Mizusaki, H.; Speziali, N. L.; Jorio, A.; Pimenta, M. A. *Carbon* **2008**, *46* (2), 272–275.
(32) Dresselhaus, M.; Jorio, A.; Hofman, M.; Dresselhaus, G.; Saito, R. *Nano Lett.* **2010**, *10* (3), 751−758.
(33) Ferrari, A. C.; Robertson, J. *Phys. Rev. B* **2000**, *61* (20), 14095.
(34) Tuinstra, F.; Koenig, J. L. *J. Compos Mater.* **1970**, *4*, 492.
(35) Tuinstra, F.; Koenig, J. L. *J. Chem. Phys.* **1970**, *53* (3), 1126.
(36) Matthews, M. J.; Pimenta, M. A.; Dresselhaus, G.; Dresselhaus, M. S.; Endo, M. *Phys. Rev. B* **1999**, *59* (10), R6585–R6588.
(37) Casiraghi, C.; Hartschuh, A.; Qian, H.; Piscanec, S.; Georgi, C.; Fasoli, A.; Novoselov, K. S.; Basko, D. M.; Ferrari, A. C. *Nano Lett.* **2009**, *9* (4), 1433–1441.
(38) Mohiuddin, T. M. G.; Lombardo, A.; Nair, R. R.; Bonetti, A.; Savini, G.; Jalil, R.; Bonini, N.; Basko, D. M.; Galiotis, C.; Marzari, N.; Novoselov, K. S.; Geim, A. K.; Ferrari, A. C. *Phys. Rev. B* **2009**, *79* (20), 205433.
(39) Casiraghi, C.; Pisana, S.; Novoselov, K. S.; Geim, A. K.; Ferrari, A. C. *Appl. Phys. Lett.* **2007**, *91* (23), 233108.
(40) Basko, D. M.; Piscanec, S.; Ferrari, A. C. *Phys. Rev. B* **2009**, *80* (16), 165413.
(41) Das, A.; Pisana, S.; Chakraborty, B.; Piscanec, S.; Saha, S. K.; Waghmare, U. V.; Novoselov, K. S.; Krishnamurthy, H. R.; Geim, A. K.; Ferrari, A. C.; Sood, A. K. *Nat. Nanotechnol.* **2008**, *3* (4), 210–215.
(42) Guinea, F.; Katsnelson, M. I.; Vozmediano, M. A. H. Physical Review B 2008, *77* (7), 075422.
(43) Cortijo, A.; Vozmediano, M. A. H. *Phys. Rev. B* **2009**, *79* (18), 184205.
(44) Xu, K.; Cao, P.; Heath, J. R.; *Nano Lett.* **2009**, *9* (12), 4446−4451.
(45) Boukhvalov, D. W.; Katsnelson, M. I. *J. Phys. Chem. C* **2009**, *113* (32), 14176–14178.
(46) Elias, D. C.; Nair, R. R.; Mohiuddin, T. M. G.; Morozov, S. V.; Blake, P.; Halsall, M. P.; Ferrari, A. C.; Boukhvalov, D. W.; Katsnelson, M. I.; Geim, A. K.; Novoselov, K. S. *Science* **2009**, *323* (5914), 610–613.
(47) Park, C. H.; Yang, L.; Son, Y. W.; Cohen, M. L.; Louie, S. G. *Nat. Phys.* **2008**, *4* (3), 213–217.

© 2010 American Chemical Society

DOI: 10.1021/nl9037714 | *Nano Lett.* **2010,** *10,* 1542--1548